Effect of Tool Temperature on Microstructure and Properties of Tailored Hot Stamping Components

Zhiqiang Zhang, Jianhao Yu, Songfeng Meng, Yong Zhao, and Dongye He

Traditional boron steel hot stamping technology can achieve components with full martensite and tensile strength of 1500 MPa. However, fully martensitic hot stamped components exhibit very low level of ductility and are rarely used in energy absorbing structures. Hot stamping with segmented heating and cooling tool can obtain multiphase quenched structures and the tailored mechanical properties. Hot stamping experiment of U-shape component was performed with segmented heating and cooling tool. Mechanical properties of the formed component were measured, and scanning electron microscope and color tint etching were used to quantify the quenched phases achieved under different tool temperatures. The results showed that hardness value decreased from 470 to 230 HV and tensile strength reduced about 50% from 1406 to 730 MPa and elongation increased from 4.19 to 10.20% as tool temperatures increased from 25 to 500 °C. Meanwhile, martensite decreased from 85 to 30% and bainite increased from 12 to 55%, and there was also a small increase in ferrite. In order to get the influence of quenched phases on the strength and hardness of tailored hot stamped component, linear fitting optimization was used to establish mathematical models for area fraction of quenched phases and strength and hardness.

1. Introduction

Hot stamping of boron steel is increasingly used in automotive industry. It can achieve full martensite structure by forming and quenching rapidly in cold tool and then get the component with tensile strength of 1500 MPa (Ref 1, 2). However, fully martensitic hot stamped components exhibit very low level of ductility and are rarely used in energy absorbing structures (Ref 3, 4). To improve the energy absorption, a hot stamped component with tailored mechanical properties is newly developed. A hot stamped B-pillar, for example, could be improved by reducing the martensite content at the lower region to improve the deformation and energy absorption, while maintaining a fully martensitic microstructure at the upper region where intrusion resistance is essential as shown in Fig. 1. According to the CCT diagram of boron steel, cooling rates less than the critical rate of 30 °C/s will result in the formation of lower strength and softer phases, such as ferrite and bainite (Ref 5). Bardelcik (Ref 6) and Li (Ref 7) have studied the influence of different cooling rates on quenching microstructure of boron steel. Increasing tool

temperature is an effective way to reduce the cooling rate. Some researchers have studied the influence of tool temperature on the properties of the hot stamped component (Ref 8-13). The results show that strength and hardness of the component decrease and ductility increases with the increase in tool temperatures. The previously mentioned studies have found the influence of tool temperature on properties but did not quantify the quenched microstructure. There are also few reports about studies on the relationship between the area fraction of quenched phases and mechanical properties at present.

Based on the deficit in published researches, hot stamping experiments were performed on boron steel U-shape component with segmented heating and cooling tool in this paper. Quenched phases under different tool temperatures could be accurately achieved to control the tailored mechanical properties. Quantitative measurement of quenched phases was conducted with scanning electron microscope and color tint etching. Tensile and hardness tests were carried out on the components with different quenched phases to get the relationship between the area fraction of microstructure and mechanical properties.

2. Experimental Study

2.1 Hot Stamping Experiments with Segmented Heating and Cooling Tool

The material used for this experiment is Usibor 1500P boron steel with a thickness of 1 mm, and the chemical composition is as follows: C, 0.22; Mn, 1.23; Si, 0.25; B, 0.004; P, 0.008; Cu, 0.03; Ni, 0.02; Cr, 0.20; Al,0.03; and Ti, 0.037. Figure 2 shows the segmented heating and cooling tool. Cooling channels were machined on the cooling tool, and the chilled water circulating in them would take away the heat from hot blank to the tool. Built-in electric cartridge heaters were installed in the heating tool to control the tool temperatures by PID system. The

Zhiqiang Zhang, Jianhao Yu, and Songfeng Meng, Key Laboratory of Automobile Materials, Ministry of Education and School of Material Science and Engineering, Jilin University, No. 5988 Renmin Street, Changchun 130025, China; and Yong Zhao and Dongye He, Key Laboratory of Automobile Materials, Ministry of Education and School of Material Science and Engineering, Jilin University, No. 5988 Renmin Street, Changchun 130025, China; and Roll Forging Research Institute, Jilin University, Changchun China. Contact e-mails: zhangzq@jlu.edu.cn, 1229112829@qq.com, 406727973@qq.com, zhao_yong@jlu.edu.cn, and dyhe_jlu@sina.com.
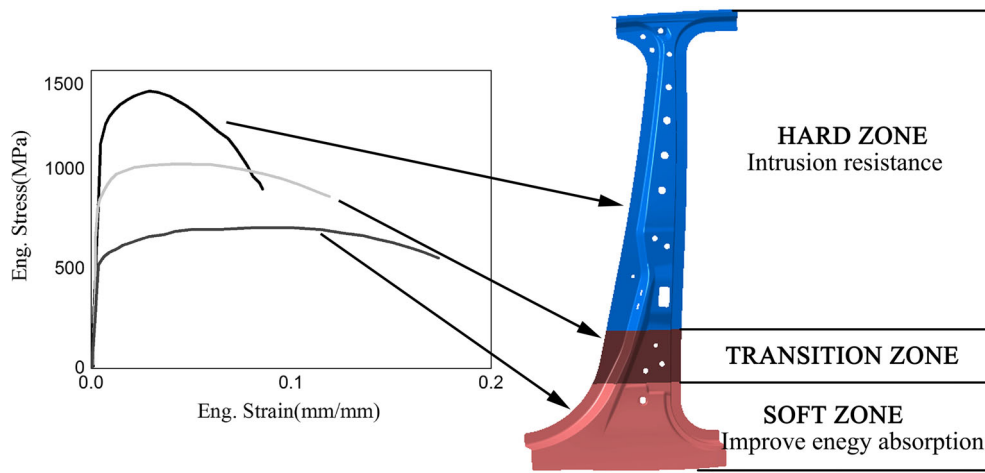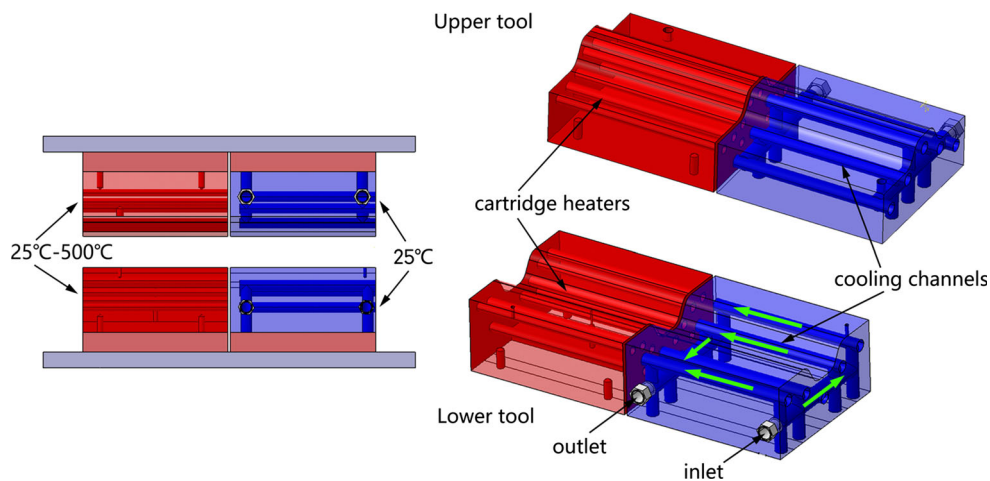
Fig. 1 B-pillar with tailored properties

Fig. 2 The tool with segmented heating and cooling

cooling tool was kept at 25 °C, while the heating tool temperatures were 25, 200, 300, 400, 450 and 500 °C, respectively. To avoid heat transfer from the heating tool to the press, 10-mm-thick asbestos cement plates were used between the tools and the press.

The blank was heated to 930 °C in the furnace and kept for 5 min. After the blank was austenized, it was removed from the furnace and transferred to the tools for forming and quenching simultaneously. Then the quenched component was removed out of the tools for air cooling to room temperature. Transferring the blank from the furnace to the tools was for 10 s, and quenching in the tools was for 10 s. Maximum load of the press was 80kN.

2.2 Metallography

The specimens of 15×6 mm were cut from the corners of cold zone and hot zone, respectively, for microstructure observation. The specimens were ground, polished and corroded with 4% nital solution. TESCAN Vega3 SEM was used to make metallographic observation of quenched phases. In order to quantify the area fractions of quenched phases, color

tint etching was used to observe the quenched phases. The specimens were put into 4% picral solution for 20 s and immediately washed and dried which was followed by putting into 10% aqueous sodium metabisulfite solution for 10 s. ZEISS Axio.Scope.A1 optical microscope was used to observe the specimens, and it was found that martensite was brown and bainite was black and ferrite was white. ImagePro Plus 7.0 software was used to calibrate martensite (green), bainite (red) and ferrite (blue) in the color metallographs and then quantify the area fractions of quenched phases.

2.3 Mechanical Properties Testing

Uniaxial tension tests were conducted on the U-shape components quenched with tool temperatures between 25 and 500 °C at the nominal strain rate 0.003 s^{-1}. The specimen size and cutting position are shown in Fig. 3. Micro-hardness measurements were made with a HVS-1000ZDT hardness tester using a 200-g load. Hardness specimens were cut from the transition zone on the top surface and have a total length of 90 mm. Measurements were taken every 2 mm and were recorded left to right.
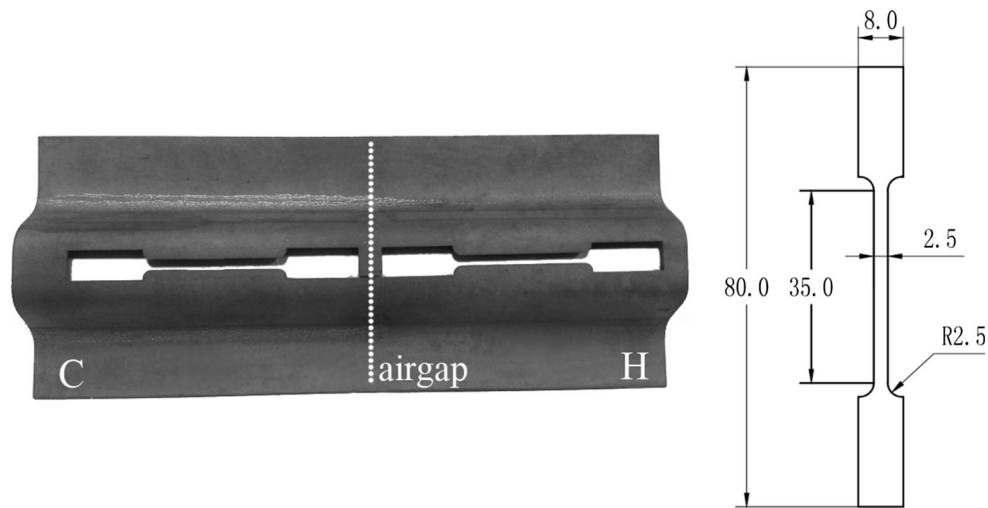
Fig. 3 The cutting locations and geometry of tension specimen

3. Results and Discussion

3.1 Metallographic Analysis Results

The temperature history of a component in cooling process has an important influence on quenched microstructures and content. It is very difficult to physically measure the temperature–time history at a point within a component during the hot stamping process. Therefore, a coupled thermal–mechanical–microstructural finite element model in LS-DYNA FE code was used to simulate the hot stamping process (transfer, forming and quenching, and air cooling). Figure 4 shows the temperature–time histories at the heating tool temperature of 25, 400 and 500 °C. Overlaid in Fig. 4 is the continuous cooling transformation (CCT) diagram of the Usibor1500P boron steel. The cooling rates are highly nonlinear; hence, the CCT is included only for discussion purposes. The 10-s transfer simulation predicts the blank temperature reduction due to convective cooling from 930 °C. The second simulation is the forming process (2 s). The third simulation is the quenching process with 10 s holding time. The final simulation is the air cooling operation after the component was removed from the tools and cooled to room temperature.

Figure 5 displays the typical microstructures of quenched components when the tool temperatures are 25, 400 and 500 °C, respectively. When the tool temperature is 25 °C, most of the quenched structures are martensite and a small amount of ferrite and bainite (refer to Fig. 5a). Martensite exhibits the packets of parallel lath crystals that are characteristic of martensite containing < 0.6% carbon (Ref 14). It is known from the temperature–time curve that the cooling rate at the tool temperature of 25 °C is far higher than the critical rate of martensite transformation. A small amount of ferrite and bainite in quenched microstructure is caused by excessive transfer time. Studies made by Barcellona (Ref 15) and Merklein (Ref 16) have shown that deformation during quenching of boron steels causes the CCT diagram to shift left or toward lower quench times, which can lead to the formation of ferrite. Figure 5b shows a martensite and bainite multiphase condition. The characteristic feature of bainite is a ferrite matrix with dispersed cementite particles (Ref 17, 18). A small amount of
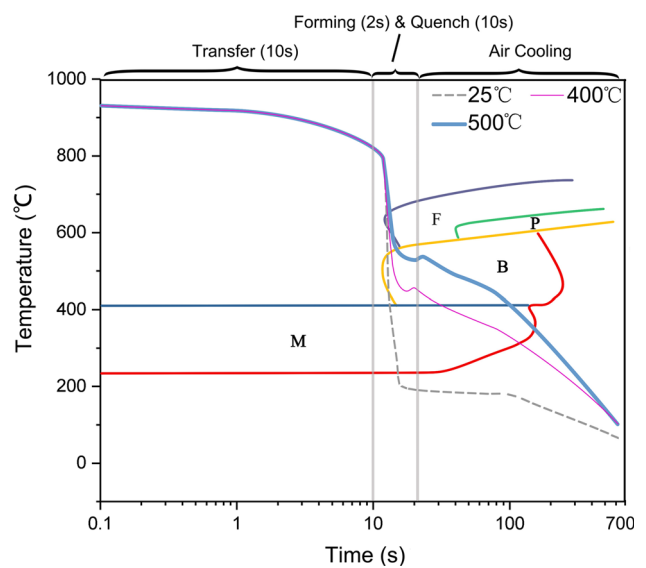

Fig. 4 The predicted temperature–time curves at the different tool temperatures. The CCT diagram is overlaid for reference only

ferrite is present in Fig. 5c and is shown by a flat and uniform structure (Ref 19).

By SEM metallographic observation and color tint etching methods, the area fractions of martensite, bainite and ferrite are determined under each tool temperatures as shown in Fig. 6. When the tool temperature increases from 25 to 500 °C, the area fraction of martensite reduces from 80 to 30% and bainite increases from 12 to 55%. The area fraction of martensite decreases slowly with the tool temperature lower than 200 °C, while the martensite content decreases obviously when the tool temperature is higher than 400 °C. The area fraction of ferrite increases slightly with the increase in the tool temperature and reaches 15% at the tool temperature of 500 °C. According to the CCT diagram, the cooling rate decreases with the increase in the tool temperature, resulting in an increase in bainite and ferrite.
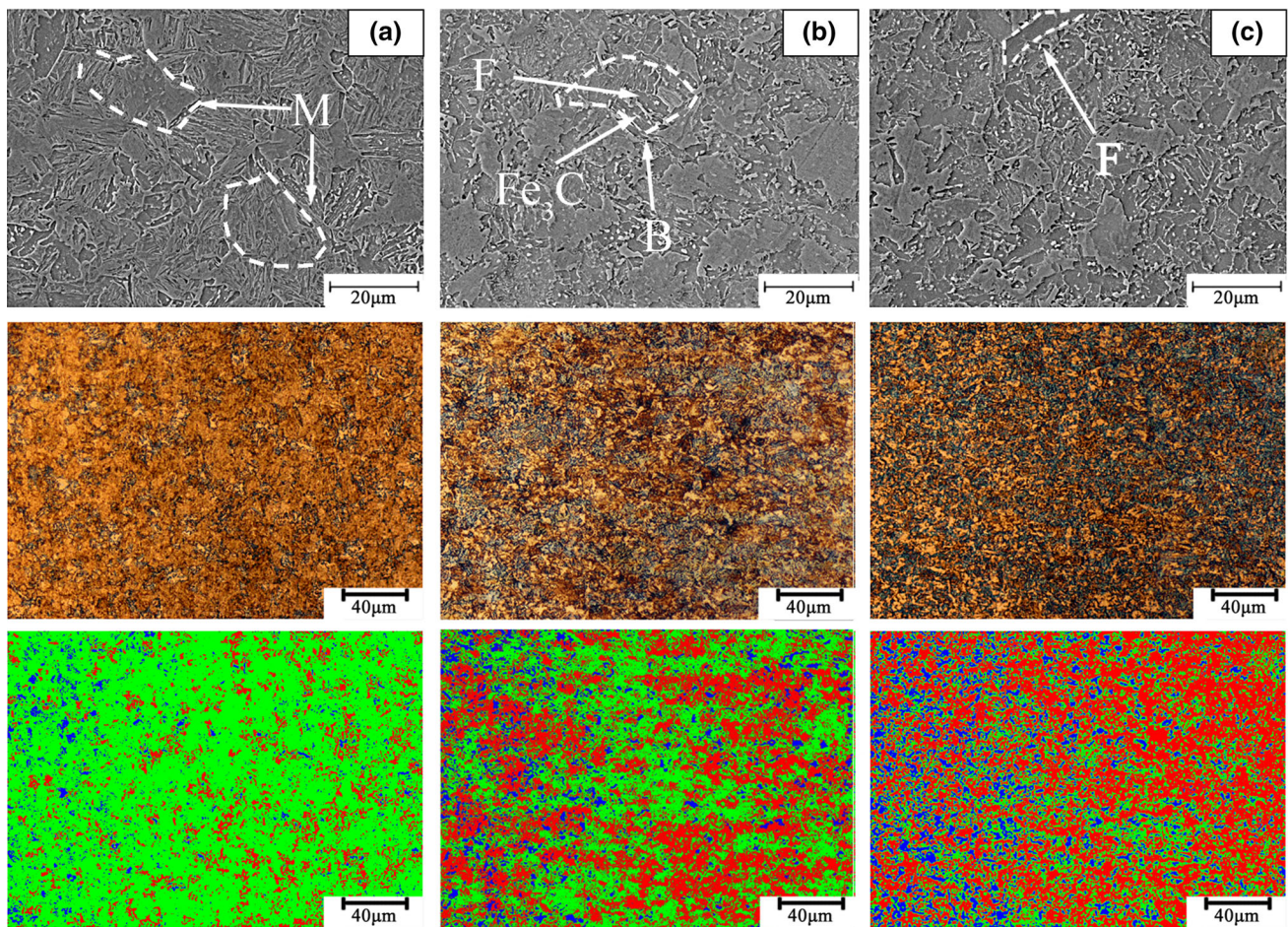
Fig. 5 Various micrographs showing (from top to bottom) the SEM images, two-stage color-etched optical micrographs and the manually generated microstructure images that were used to quantify the area fractions of quenching phases at the tool temperature of (a) 25 °C, (b) 400 °C, and (c) 500 °C
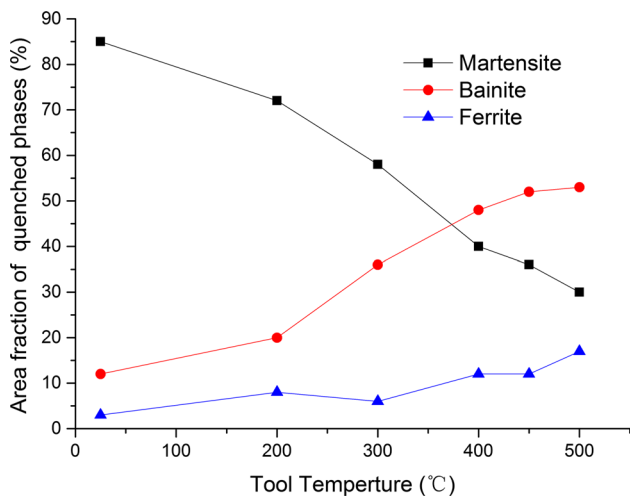

Fig. 6 Area fractions of quenched phases under different tool temperatures

Fig. 7 Stress–stain curves under different tool temperatures

3.2 Relationship Between Quenched Phases and Strength and Hardness

Stress–strain curves at different tool temperatures are shown in Fig. 7 (C for cold zone and H for hot zone). The values of
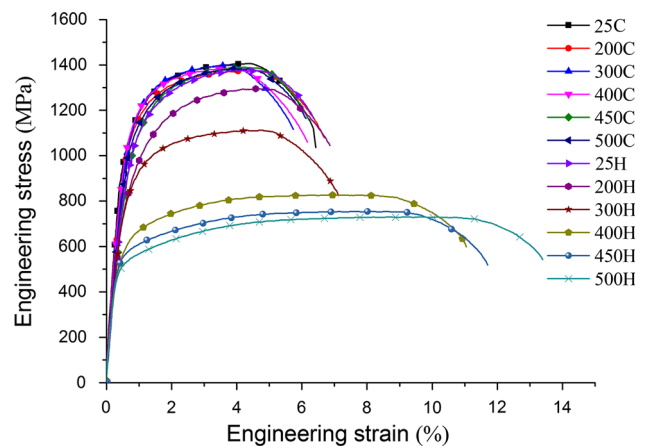
yield strength (YS), ultimate tensile strength (UTS) and elongation are listed in Table 1. Since the geometry of specimen is not the standard one of ASTM, the elongation at the UTS was used instead of the elongation at failure. The YS and UTS in cold zone are over 900 and 1300 MPa, respectively, and the elongation is about 4% no matter how the heating tool temperature is changed. High strength and low

Table 1 Values of YS, UTS and elongation at different tool temperatures

Sample	YS, MPa	UTS, MPa	Elongation, %
25C	956	1406	4.48
200C	931	1377	4.61
300C	948	1400	3.88
400C	945	1386	4.07
450C	950	1390	4.29
500C	943	1384	3.97
25H	937	1378	4.21
200H	849	1296	4.67
300H	834	1112	4.82
400H	627	826	7.90
450H	543	754	8.68
500H	508	730	10.22

ductility of cold zone is due to its almost full martensite structure. With the increase in tool temperatures, the YS and UTS in the hot zone reduce dramatically, while the elongation increases. The UTS reduces to the lowest 730 MPa and the elongation reaches the maximum of 10.20% when the heating tool temperature is 500 °C. The reason is that the area fraction of martensite reduces and that of bainite increases with the increase in heating tool temperature.

An assessment of the fracture behavior for the different tool temperatures was conducted through metallographic observation of the tensile fracture surfaces using optical microscope and SEM as shown in Fig. 8. The specimen exhibits shear fracture behavior when the tool temperature is 25 °C. The fracture surface is planar, and large surface cracks surrounded by small fibrous regions with very shallow dimples confirm the shear fracture mechanism (refer to Fig. 8a). Figure 8b and c shows the classic cup and core fracture surface which indicates ductile fracture behavior when the tool temperature is higher
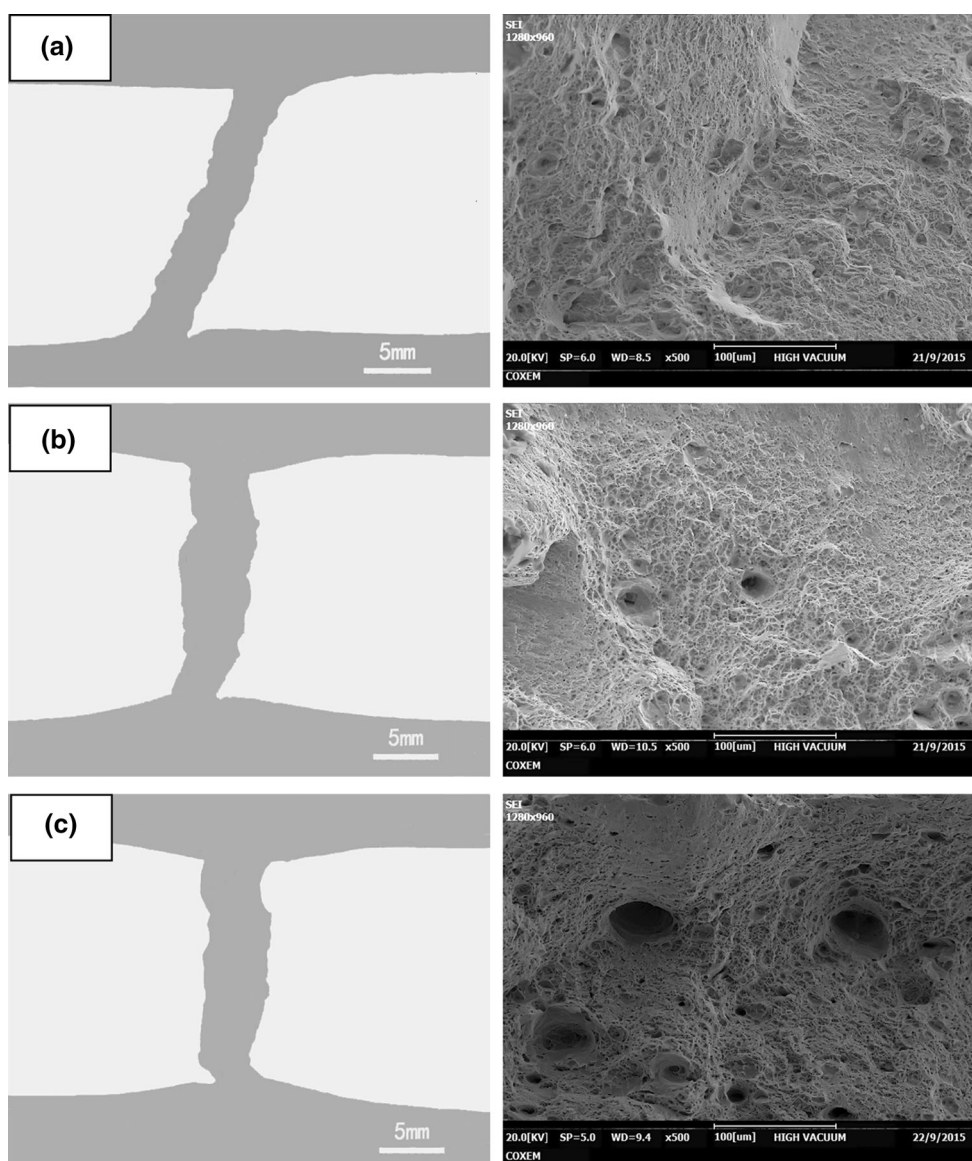

Fig. 8 Optical microscope images and SEM images of fracture surfaces at the tool temperature of (a) 25 °C, (b) 400 °C and (c) 500 °C

than 400 °C. Well-defined and deep dimples are also shown in the higher-magnification SEM images. The fracture surface presents dark gray at the tool temperature of 500 °C because the deeper dimples resulting in the decrease in the light reflection ability.

Figure 9 shows the relationship between the UTS and area fractions of martensite and bainite. Ferrite is not considered for its less amount. It is found that the UTS increases with the increase in martensite and shows a positive linear correlation. The UTS drops with the increase in bainite and presents a negative linear correlation. With the UTS as the dependent variable and the area fractions of martensite and bainite as the independent variable, the multiple linear regression analysis was carried out and the goodness-of-fit R-squared value is 0.983. The result shows that there is a strong linear relationship between UTS and area fractions of martensite and bainite. A linear trendline was fit to the data and is shown as equation UTS = $1.7 \times (1512.9 \times M + 1114.5 \times B) - 1075.3$.

Figure 10 shows the longitudinal hardness distribution at the top of the U-shape component. It can be seen that hardness drops as tool temperatures increase. When tool temperature is at 25 °C, the hardness value is the highest 470 HV. Åkerström and Oldenburg (Ref 20) found the hardness value of martensite is 510 HV. As the quenched components contain a small amount of ferrite and bainite, the hardness is lower than that of martensite. The hardness values range from 200 to 300 HV as the tool temperature is higher than 400 °C and reach the lowest 230HV at the tool temperature of 500 °C. When the tool
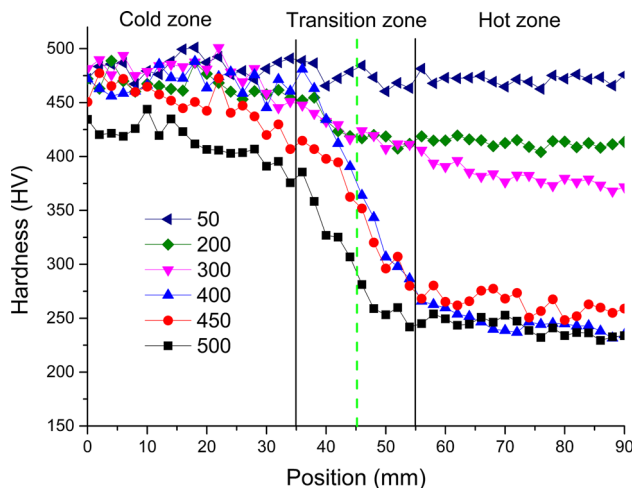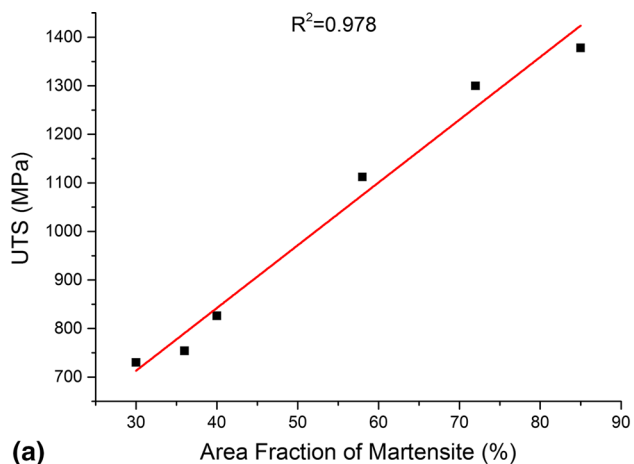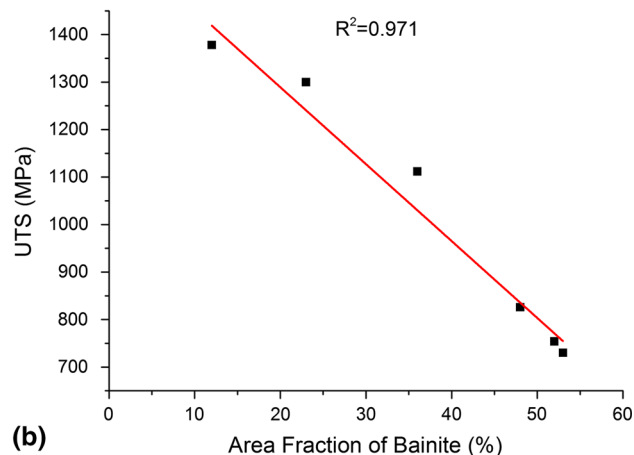
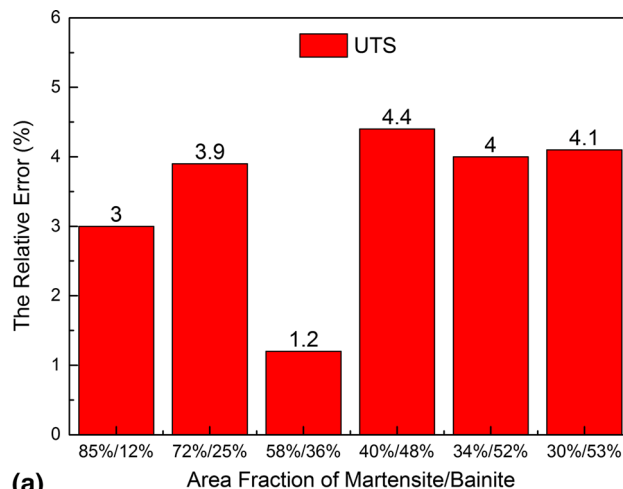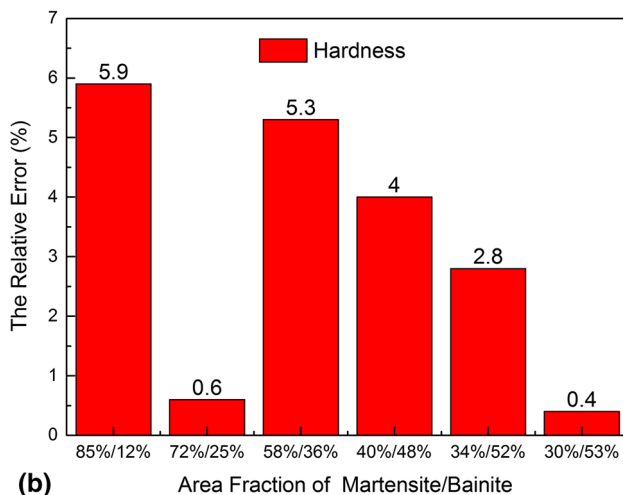**Fig. 10** Longitudinal hardness distribution under different tool temperatures

Fig. 9 Relationship between UTS and area fraction ratio of (a) martensite and (b) bainite

Fig. 11 Relative errors of calculated and measured values of (a) UTS and (b) hardness

Table 2 Comparison of experimental and calculated values

Cooling rate, °C/S	Area function martensite/bainite	UTS Exp., MPa	UTS Cal., MPa	HV Exp.	HV Cal.
14	3%/97%	816	839	272	267
17	12%/88%	929	900	283	288
24	57%/43%	1203	1205	392	394
28	86%/14%	1360	1401	449	463
50	97%/3%	1447	1476	472	489

temperatures are higher than 400 °C, the dramatic drop of hardness is due to the decrease in cooling rate caused by the high tool temperature. High cooling rate in the quenching process can lead to high hardness (Ref 21-24). When the tool temperature is over 400 °C, the component temperature at the end of the quench period is higher than the bainite transformation finish temperature of 460 °C (Ref 25). The reducing cooling rate after the component was removed from the tool causes the increase in bainite and the decrease in martensite, which leads to the significant decrease in the hardness.

Multiple linear regression analysis was carried out between the hardness and the area fractions of martensite and bainite. The R-squared value is 0.989. Linear fitting optimization was conducted, and the model is shown as $HV = 40.2 \times (20.4 \times M + 14.6 \times B) - 326.5$.

Figure 11 shows the relative errors of calculated and measured values of the UTS and hardness under different area fractions of martensite and bainite. It can be found that the maximum relative error is $< 6\%$, which indicates the high reliability of the UTS and the hardness calculated by the established models. Those models can be used to accurately predict the strength and hardness of the hot stamped components based on the area fractions of quenched phases.

In order to investigate the application scope of the model, the data of UTS and hardness with different area fractions of martensite and bainite in the literature (Ref 6) were used to verify. Compared to the multi-segment nonlinear cooling (transfer, forming and quenching, and air cooling) in this paper, the cooling path in the literature (Ref 6) is continuous under forced air. Table 2 displays the calculated values and experimental values of UTS and hardness. It can be seen that the calculated values obtained by the models under continuous cooling condition are in good agreement with the experimental values.

4. Conclusion

Hot stamping experimental device with segmented heating and cooling tool was developed in this paper to conduct experiments with tool temperatures of 25-500 °C and get components with tailored mechanical properties. Microstructure analyses and mechanical property tests were carried out on the components, and the following conclusions can be drawn:

(1) Hot stamping component with tailored mechanical properties could be obtained with segmented heating and cooling tool. There was a noticeable change in mechanical properties of the component especially when tool temperature was higher than 400 °C.

(2) Results from SEM and color tint etching showed that martensite reduced, while bainite and ferrite increased as tool temperatures increased. It was found that martensite reduced from 85 to 30% and bainite increased from 12 to 55% and ferrite increased from 4 to 15% as tool temperatures rose from 25 to 500 °C. When the tool temperature was 400 °C, the area fraction of bainite was more than that of martensite.

(3) Tensile results showed that the highest UTS of 1406 MPa appeared at tool temperature of 25 °C. With the increase in tool temperatures, the UTS reduced and the elongation increased. The UTS was 730 MPa, a reduction of 50%, while elongation increased by 143% at tool temperature of 500 °C. Hardness values were 470HV and 230HV, respectively, at tool temperatures of 25 and 500 °C.

(4) UTS and Vickers hardness were approximately linear correlation with area fraction of martensite and almost negative linear with bainite content. Linear fitting optimization of experimental data was conducted to obtain mathematical models of the UTS, hardness and area fractions of martensite and bainite.

References

1. H. Karbasian and A.E. Tekkaya, A Review on Hot Stamping, *J. Mater. Process. Technol.*, 2010, **210**, p 2103–2118
2. Y.H. Shen, Y.L. Song, L. Hua, and J. Lu, Influence of Plastic Deformation on Martensitic Transformation During Hot Stamping of Complex Structure Auto Parts, *J. Mater. Eng. Perform.*, 2017, **26**(4), p 1830–1838
3. W.H. Lin, F. Li, D.S. Wu, X.G. Chen, X.M. Hua, and H. Pan, Effect of Al-Si Coating on Weld Microstructure and Properties of 22MnB5 Steel Joints for Hot Stamping, *J. Mater. Eng. Perform.*, 2018, **27**(4), p 1825–1836
4. M. Merklein, M. Wieland, M. Lechner, S. Bruschi, and A. Ghiotti, Hot Stamping of Boron Steel Sheets with Tailored Properties: A Review, *J. Mater. Process. Technol.*, 2016, **228**, p 11–24
5. M. Naderi, L. Durrenberger, A. Molinari, and W. Bleck, Constitutive Relationships for 22mnb5 Boron Steel Deformed Isothermally at High Temperatures, *Mater. Sci. Eng., A*, 2008, **478**, p 130–139
6. A. Bardelcik, M.J. Worswick, S. Winkler, and M.A. Wells, A Strain Rate Sensitive Constitutive Model for Quenched Boron Steel with Tailored Properties, *Int. J. Impact Eng*, 2012, **50**, p 49–62
7. F.F. Li, M.W. Fu, and J.P. Lin, Effect of Cooling Path on the Phase Transformation of Boron Steel 22mnb5 in Hot Stamping Process, *Int. J. Adv. Manuf. Technol.*, 2015, **81**, p 1391–1402
8. K. Omer, L. Kortenaar, C. Butcher, M. Worswick, S. Malcolm, and D. Detwiler, Testing of a Hot Stamped Axial Crush Member with Tailored

Properties Experiments and Models, *Int. J. Impact Eng*, 2017, **103**, p 12–28

9. M.B. Zhou, J.L. Tang, J. Yang, and C.Y. Wang, Tailored Properties of a Novelly Designed Press Hardened 22MnMob Steel, *J. Iron. Steel Res. Int.*, 2017, **24**, p 508–512

10. Y.H. Mu, B.Y. Wang, J. Zhou, X. Huang, and X.T. Li, Hot Stamping of Boron Steel Using Partition Heating for Tailored Properties: Experimental Trials and Numerical Analysis, *Metall. Mater. Trans. A*, 2017, **48**, p 5467–5479

11. Y.H. Mu, B.Y. Wang, J. Zhou, Y. Kang, and X.T. Li, Heating Parameters Optimization of Hot Stamping by Partition Heating for Tailored Properties, *ISIJ Int.*, 2017, **57**(8), p 1442–1450

12. R. George, A. Bardelcik, and M.J. Worswick, Hot Forming of Boron Steels Using Heated and Cooled Tooling for Tailored Properties, *J. Mater. Process. Technol.*, 2012, **212**, p 2386–2399

13. R. George, Hot Forming of Boron Steels with Tailored Mechanical Properties: Experiments and Numerical Simulation. Master thesis, University of Waterloo, 2011

14. J.P. Naylor, Influence of the Lath Morphology on the Yield Stress and Transition-Temperature of Martensitic-Bainitic Steels, *Metall. Trans. A*, 1979, **10**(7), p 861–873

15. A. Barcellona and D. Palmeri, Effect of Plastic Hot Deformation on the Hardness and Continuous Cooling Transformations of 22mnb5 Microalloyed Boron Steel, *Metall. Mater. Trans. A*, 2009, **40**(5), p 1160–1174

16. M. Merklein and T. Svec, Transformation Kinetics of the Hot Stamping Steel 22mnb5 in Dependency of the Applied Deformation on the Austenitic Microstructure, in *IDDRG 2010 International Conference* (2010), Graz, Austria, p 71–80

17. C. Feng, H. Fang, Y. Zheng, and B. Bai, Mn-series Low-carbon Air-Cooled Bainitic Steel Containing Niobium of 0.02%, *J. Iron. Steel Res. Int.*, 2010, **17**(3), p 53–58

18. H. Bhadeshia and J.W. Christian, Bainite in Steels, *Metall. Trans. A*, 1990, **21**(4), p 767–797

19. D.W. Fan, H.S. Kim, and B.C. De Coomman, A Review of the Physical Metallurgy Related to the Hot Press Forming of Advanced High Strength Steel, *Steel Res. Int.*, 2009, **80**(3), p 241–249

20. P. Åkerström and M. Oldenburg, Austenite Decomposition During Press Hardening of a Boron Steel-Computer Simulation and Test, *J. Mater. Process. Technol.*, 2006, **174**, p 399–406

21. E. Caron, K.J. Daun, and M.A. Wells, Experimental Characterization of Heat Transfer Coefficients During Hot Forming Die Quenching of Boron Steel, *Metall. Mater. Trans. B*, 2013, **44**, p 332–343

22. J. Mendiguren, R. Ortubay, E.S. Argandoña, and L. Galdos, Experimental Characterization of the Heat Transfer Coefficient under Different Close Loop Controlled Pressures and Die Temperatures, *Appl. Therm. Eng.*, 2016, **99**, p 813–824

23. Z.Q. Zhang, P. Gao, C.H. Liu, and X.J. Li, Experimental and Simulation Study for Heat Transfer Coefficient in Hot Stamping of High-Strength Boron Steel, *Metall. Mater. Trans. B*, 2015, **46**, p 2419–2422

24. A. Bardelcik, C. Salisbury, S. Winkle, M.A. Wells, and M.J. Worswick, Effect of Cooling Rate on the High Strain Rate Properties of Boron Steel, *Int. J. Impact Eng*, 2010, **37**, p 694–702

25. A. Turetta, Investigation of Thermal, Mechanical and Microstructural Properties of Quenchable High Strength Steels in Hot Stamping Operation. Master thesis, University of Padova, 2008